Benabdelaziz, Kawtar; Lebrouhi, Badreddine; Maftah, Anas; Maaroufi, Mohammed

Article

Novel external cooling solution for electric vehicle battery pack

Energy Reports

Provided in Cooperation with:
Elsevier

Suggested Citation: Benabdelaziz, Kawtar; Lebrouhi, Badreddine; Maftah, Anas; Maaroufi, Mohammed (2020) : Novel external cooling solution for electric vehicle battery pack, Energy Reports, ISSN 2352-4847, Elsevier, Amsterdam, Vol. 6, Iss. 3, pp. 262-272, https://doi.org/10.1016/j.egyr.2019.10.043

Available online at www.sciencedirect.com
ScienceDirect
Energy Reports 6 (2020) 262–272
www.elsevier.com/locate/egyr

Tmrees, EURACA, 04 to 06 September 2019, Athens, Greece

Novel external cooling solution for electric vehicle battery pack

Kawtar Benabdelaziz*, Badreddine Lebrouhi, Anas Maftah, Mohammed Maaroufi

Mohammadia School of Engineering, Mohammed V University of Rabat, Rabat 10000, Morocco

Received 19 September 2019; accepted 28 October 2019

Abstract

The future use of electric vehicles in the southern regions of the world could face several problematics related to high temperature, mostly when charging at high power. This paper proposes a new external cooling solution for cooling EV batteries pack at higher temperature conditions especially for those without effective cooling system embedded. A 3D-thermal model has been developed in order to investigate and to analyse the temperature distribution over the battery pack, the ANSYS FLUENT software has been used to solve the model development. Furthermore, different external cooling solutions have been proposed by using the engineering process design to study their impact on the internal temperature of the battery pack.

Peer-review under responsibility of the scientific committee of the Tmrees, EURACA, 2019.

Keywords: Thermal model; Batteries; Electric vehicle; Finite volume method; Response surface method; ANSYS FLUENT

1. Introduction

Recently, greenhouse gas emissions and the depletion of natural resources have become a major global problem [1], transportation is the most growing factor of the world's fuel consumption taking up 49% of oil resources [2], it is also estimated that if oil consumption follows current trends, global oil resources will be depleted by 2038 [1]. These concerns encourage automotive researchers and engineers to focus on the development of various energy sources as well as electric vehicles [3].

The electrification of transport involves incorporating, more or less massively, a reversible electrical storage system within the vehicles. Today, lithium-ion batteries have made their mark in the transport sector, mainly because of their very good energy density performance. However, despite these undeniable advantages, this technology, when used in the automotive field, suffers from certain defects: low battery life, high recharge time, high costs, etc. Another major problem is their inefficiency when the operating temperature is too high, which results in the reduction of available energy and a decrease in their life.

Battery thermal management is therefore required to help the battery operate at a desirable working temperature range at all times preventing battery degradation [4,5], thermal runaway [6,7], and loss of loads [8]. Thermal management strategies can be internal, or external, passive (only ambient air is used) or active (an integrated source

* Corresponding author.
E-mail address: kawtarbenabdelaziz@gmail.com (K. Benabdelaziz).

https://doi.org/10.1016/j.egyr.2019.10.043

Peer-review under responsibility of the scientific committee of the Tmrees, EURACA, 2019.

provides heating and/or cooling), or categorized according to the transfer medium [9–11]; either by air, liquid, or phase change material, by the heat pipes or any combination.

The operating temperature is not a factor without consequences in the cities where the summer is rough. In this context, the study made previously by [12], has shown a lack of cooling when the ambient temperature is too high (48 °C), which can reduce battery performance and lifetime [13–15]. Recently, many researchers (J. Smith [16], A. Jarrett [17], L. W. Jin [18] and W. van Gils [19]) are interested in the development and the optimization of the cold plate in order to minimize the pressure drop and maximize the removal heat and temperature uniformity.

In this paper, a novel external solution of cooling the battery pack while the vehicle is parked is presented. The first steps are the investigation of the thermal behaviour of the battery module in order to model the thermal behaviour of the battery pack in Section 3, using the finite volume method. Section 4 present the proposed solution and the different designs proposed in order to optimize the energy flow provided by the external cooling system. Extended numerical models are developed to simulate the existing cold plate's designs in order to predict the optimal architecture design which allows to decrease the temperature and to obtain a more uniform temperature distribution over the battery pack. This comparison is carried out by using the same cold plate's designs at the same conditions. In addition, the influences of liquid inlet temperature, liquid mass flow rate are also analysed. Finally, Section 5 conclude the paper.

2. Investigation of the thermal behaviour of the battery module

2.1. Characteristics of the battery

This study is devoted to the Renault Zoe battery pack (Fig. 1), which consists of 192 soft pouch cells, arranged in series and in parallel configuration. The dimensions of each module are: 373 L × 204 W × 140 H which consists of 16 cells with a 2P 8S configuration. Each cell has as dimensions: 325 × 135 × 11.2 mm, and a capacity of 35 Ah.

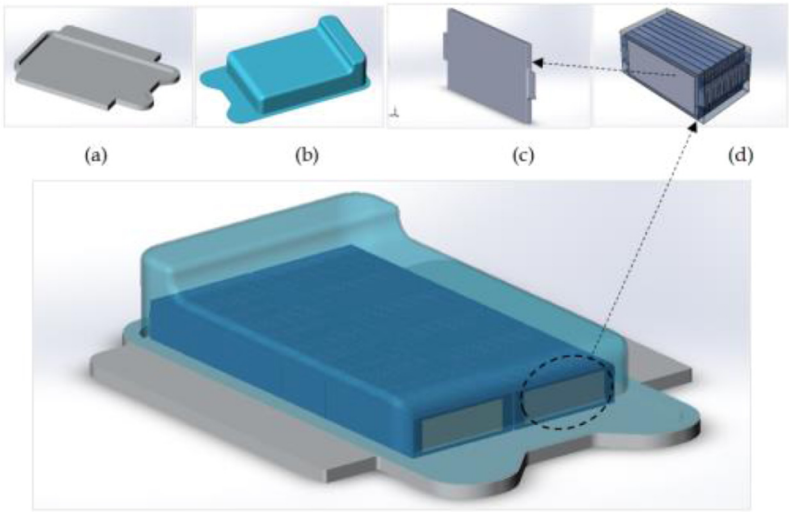

Fig. 1. (a) chassis (b) cover, (c) cellule, (d) Module (e) battery pack.

The LiFePO4/graphite lithium-ion pouch cell is made with different domains (electrode, cathode and anode) made of different materials, taking into account a thickness of 11, 2 mm for each.

2.2. Temperature distribution in lithium-ion batteries pack

In order to model the thermal behaviour of the pack, the behaviour of each module was first modelled by deducing the heat flow generated by each module (Fig. 2). The heat development in the y-direction can be neglected [20]. Thus, a two-dimensional transient heat conduction equation is sufficient to describe the thermal phenomena in the

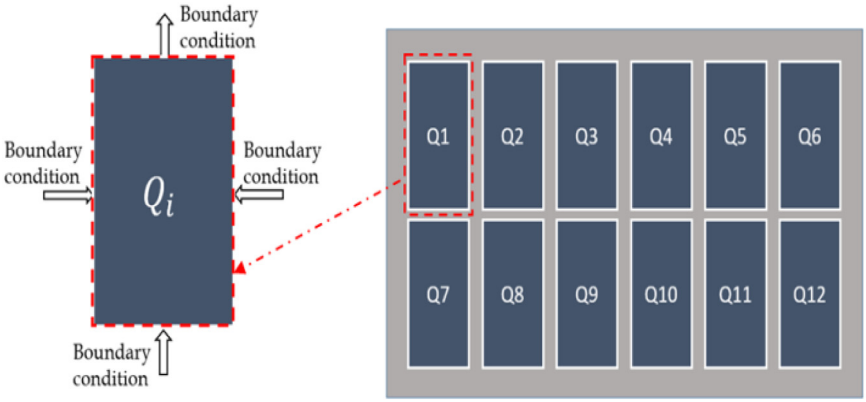

Fig. 2. Decomposition of the heat sources in the battery pack.

battery module. However the convective term inside each cell of the battery (electrode–electrolyte) can generally be neglected [21]. Therefore, the thermal conductivity is anisotropic, with a higher value along the x and z-directions, than the normal direction to the layers. Furthermore, the thermal conductivity along x-direction is the same than the z-direction.

2.3. Model development

The behaviour of the battery is investigated by using 2D-thermal model, however, the heat source in each lithium-ion battery cell has mainly three contributions: the reaction heat (q_{rea}) the reversible heat (q_{act}) and the electrical ohmic heat (q_{ohm}). The 2D-thermal model requires as inputs the thermal parameters as estimated in Table 1.

Table 1. Thermal analysis parameters.

Material proprieties	Value
Cell	Lithium-ion
Cell specific heat ($JKg^{-1}k^{-1}$)	1027
Thermal conductivity of cell in x and z-direction ($Wm^{-1}k^{-1}$)	25
Thermal conductivity of cell in y-direction ($Wm^{-1}k^{-1}$)	1
Rate of heat generation ($kW\,m^{-3}$)	22.5
Density of cells ($Kg\,m^{-3}$)	4035

The temperature of a single cell in the battery module can be calculated by the general conservation energy:

$$\rho_i C_{p,i} \frac{dT}{dt} - \lambda_i \nabla^2 T = Q_{Total,i} \tag{1}$$

where ρ_i (kg/m^3) is the density of each cell, $C_{p,i}$ $\left(jkg^{-1}K^{-1}\right)$ is the specific heat capacity of each cell, λ $\left(Wm^{-1}K^{-1}\right)$ is the thermal conductivity of the battery cell, $Q_{Total,i}$ $\left(Wm^{-3}\right)$ is the heat source generated by the cell, and T (K) is the temperature of the battery. The total heat source generated by each cell ($Q_{\boldsymbol{Total},i}$) is given by:

$$Q_{Total,i} = q_{reac,i} + q_{act,i} + q_{ohm,i} \tag{2}$$

where $q_{rea,i}$ $\left(Wm^{-3}\right)$ is the reaction heat, $q_{act,i}$ $\left(Wm^{-3}\right)$ the activation heat, and $q_{ohm,i}$ $\left(Wm^{-3}\right)$ the ohmic heat. These 3 parameters can be computed from the electro-chemical model as estimated in Table 1. In addition to heat generation in the battery pack, there are different heat dissipation mechanisms in a battery cell; heat conduction and heat convection. As the cell is an opaque system, the radiation heat transfer inside the battery pack is insignificant.

The boundary conditions are given by the balance between the conductivity heat flux from the battery module to the surroundings and the contribution of convection heat:

$$\lambda_i \nabla T = h_{conv} \left(T_{external} - T\right), i \tag{3}$$

$$\lambda_i \left(\frac{\partial T}{\partial x} + \frac{\partial T}{\partial y} \right) |_{boundaries} = h_{conv} \left(T_{external} - T \right), i \tag{4}$$

where h_{conv} ($\mathrm{Wm^{-2}K^{-1}}$) represent the convective heat transfer, T the battery surface temperature and $T_{external}$ is the external temperature. Knowing the heat generation variation and thermal parameters, finite volume numerical method is used to solve the energy balances by ANSYS Fluent software.

2.4. Results and discussion

All equations are solved numerically by ANSYS FLUENT software by using the Finite Volume Method (FVM). Indeed, domain is discretized onto a finite a set of control volumes, and the general conservation equations for energy are solved on this set of control volumes. Since the equations are nonlinear, the performance and efficiency of the calculation depend on the mesh and solver. A structured mesh is generated with CFD Fluent. To ensure the accuracy and the mesh independency of the solutions, 13,160 structured elements are used over the entire computational domain after testing several grid densities with refining zones.

The temperature is determined by using the Semi-Implicit Method for Pressure-Linked Equations Solver Algorithm. For each time step, the convergence is reached where the relative tolerance is below than 10^{-3} for all variables. Then, the time step progresses until the cut-off potential is reached.

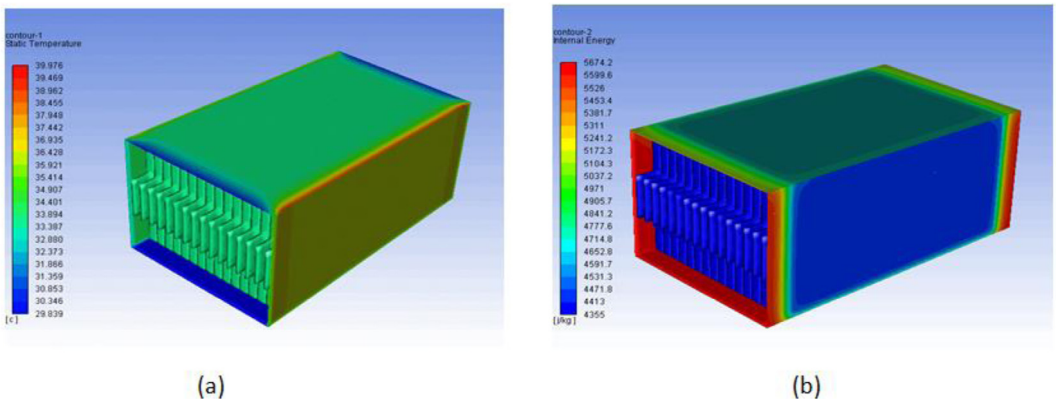

Fig. 3. (a) Temperature distribution over the battery Module; (b) The energy content in the battery module.

The Fig. 3(a) and (b) show respectively the temperature distribution and the energy content in the battery module at high discharge rate. In fact, it indicates that the battery surface temperature is nearly uniform, except in the side wall where the maximum temperature is (39,975 °C). The battery module temperature rises more by time, due to the increase of the heat generation in the electrodes and tab domains.

3. Investigation of the Thermal behaviour of the battery pack

3.1. Model development

The thermal behaviour of the pack is investigated by using the thermal model as used for the battery module. Indeed, the battery modules have been considered as heat sources with a maximum heat generated (5134 $\mathrm{Wm^{-3}}$). Moreover, the investigation's result of the thermal behaviour of each module has been used as thermal parameters inputs (see Fig. 4).

The temperature of the battery pack can be calculated by the general conservation energy equation which is formulated as:

$$\rho_j C_{p,j} \frac{dT}{dt} - \lambda_j \nabla^2 T = Q_j \tag{5}$$

where $\rho_j(\mathrm{kg/m^3})$ is the density of each module, $C_{p,j}$ $\left(\mathrm{jkg^{-1}K^{-1}}\right)$ is the specific heat capacity of each module, λ $\left(\mathrm{Wm^{-1}K^{-1}}\right)$ is the thermal conductivity of the battery module, Q_j $\left(\mathrm{Wm^{-3}}\right)$ is the rate of heat generated by the module, and T (K) is the temperature of the battery.

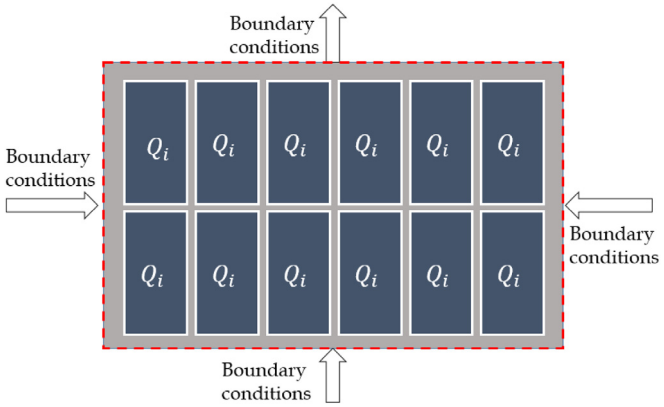

Fig. 4. Heat source generation in the battery pack and the boundary conditions.

The boundary conditions are given by the balance between the conductivity heat flux from the battery pack surface to the surroundings and contribution of convection heat.

$$\lambda_j \nabla T = -h_{conv} \left(T_{external} - T\right), j \tag{6}$$

$$\lambda_j \left(\frac{\partial T}{\partial x} + \frac{\partial T}{\partial y} + \frac{\partial T}{\partial z}\right)|_{boundaries} = -h_{conv} \left(T_{external} - T\right) \tag{7}$$

3.2. Results and discussion

The equations are solved by using the same method as used for the battery module. To ensure the accuracy and the mesh independency of the solutions, 1,108,273 structured elements are used over the entire computational domain after testing several grid densities with refining zones as shown in Fig. 5(a).

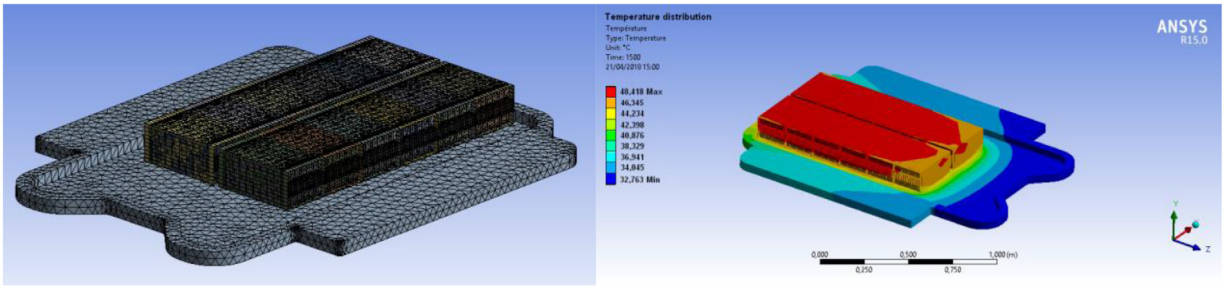

Fig. 5. (a) Meshing of battery packs; (b) Temperature distribution in the battery pack.

Fig. 5(b) shows the temperature distribution over the battery pack at high discharge rate. It indicates that the battery surface temperature is nearly uniform, except in the middle where the maximum temperature is located (48 °C). This value is higher than the recommended operation value in the charging state [22], in fact and external cooling system is required to reduce it.

4. Investigation of the proposed solution's designs

Sections 2 and 3 showed that the battery is affected by the temperature of the chassis, that can easily rise at high ambient temperature. As the heat transfer to the battery pack is made possible through the chassis, the proposed solution is to place a cold plate directly in contact with it, as shown in Fig. 6. The battery pack is then cooled by conduction when in contact. The cold plate includes one or more internal channel through which a liquid is flowing, in order to increase the cooling efficiency and reduce the amount of liquid and the power consumption. The heat is generated by the battery, transferred into the cold plate, and removed throughout the cooling channels. This system is generally used in a smaller range for cooling cells in each module [23].

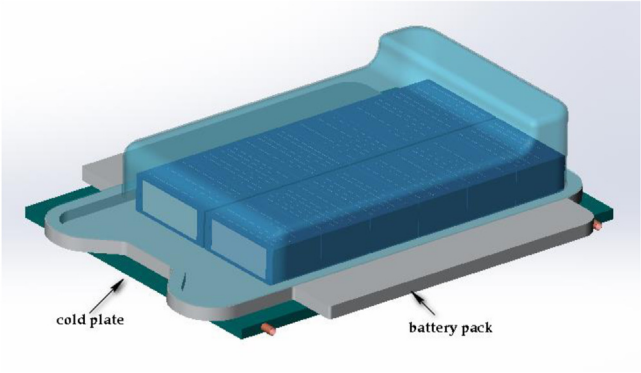

Fig. 6. The external cooling plate place under the battery pack.

4.1. Model assumptions and geometry features

Four cold plates' designs are investigated in order to illustrate the most efficient in terms of the maximum temperature rising and temperature distribution of the battery pack. The overall system is insulated in order to quantify the effectiveness's of the different cold plate designs and to represent the real situation in pack level where the battery is covered by protective material. The cooling plate and cooling channel are made of aluminium and copper, respectively. The schematics of the different cold plate's designs are represented in Fig. 7 and have the same dimensions of 1630 mm in length, 1200 mm in width and 40 mm in thickness. The different cold plate designs differ from the structure of the cooling channels with an inner diameter of 30 mm:

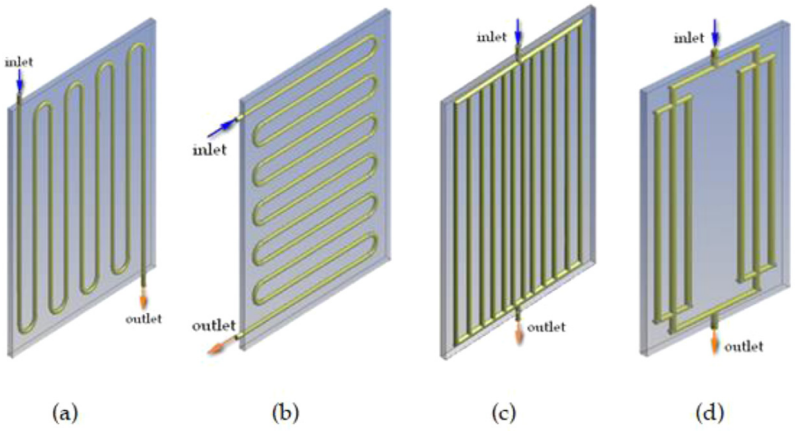

Fig. 7. Different cooling plate designs: (a) design 1; (b) design 2; (c) design 3; (d) design 4.

Design 1 comprises one cooling channel having an inlet and outlet ends on the left side of the cold plate, the intermediate portion with a sinuous arrangement horizontally; this design has the advantage of conducting the total flow rate into the cooling channel. However, the second design has the same characteristic as the design 1, except the intermediate portion which arranged vertically. The design 3 is characterized by 12-straight cooling channels distributed equidistantly along the width of the cold plates; the inlet connector channel is placed at the middle in order to have more flow rate at the middle of the cold plate. The outlet connector channel is placed at the middle of the bottom to recover the hot liquid. This design has the advantage of reducing the pressure drop inside the cooling channel. Finally, the design 4 is characterized by 6-straight cooling channels, where the total flow rate is split uniformly into the different lines.

The simulation of heat transfer of the full system requires a 3D geometry representation, while the simulation of 3D flow and heat transfer inside the cooling channels is expensive. As the diameter of the cooling channel is

smaller (30 mm) the flow and heat transfer inside the cooling channels can be modelled with 1D pipe thermal-flow equations coupled with the 3D modelling of the cold plates [23]. The equations describing the cooling channel flow are fully coupled with the heat transfer equations of the cooling plate and the battery pack.

4.2. Governing equations

The energy equation for the energy balance is given by:

$$\rho C_p \frac{\partial T}{\partial t} = \lambda \nabla^2 T \tag{8}$$

where $\rho\left(\mathrm{kg/m^3}\right)$ the density of the cold plate is, $C_p\left(\mathrm{jkg^{-1}K^{-1}}\right)$ is the specific heat capacity of the cold plate, $\lambda\left(\mathrm{Wm^{-1}K^{-1}}\right)$: is the thermal conductivity of the cold plate, made of aluminium.

For the Flow and heat transfer in the cooling channels, the momentum and mass conservation of the 1D pipe flow in the cooling channels describes below are a simplified form of the Navier–Stokes equations:

$$\rho \frac{\partial v}{\partial t} = -\nabla p - f_D \frac{\rho}{2d_h} |v|\, v + F_{gravity} \tag{9}$$

$$\frac{\partial A\rho}{\partial t} + \nabla \cdot (A\rho v) = 0 \tag{10}$$

where v (m/s) is the averaged fluid velocity at the cross section of the cooling channel, $A\left(\mathrm{m^2}\right)$ is the cross section of the cooling channel, d_h (m) is the hydraulic diameter of the cooling channel, $\rho\left(\mathrm{kg/m^3}\right)$ is the density of the water ethylene glycol, $p\left(\mathrm{N/m^2}\right)$ is the pressure, $F_{gravity}\left(\mathrm{N/m^3}\right)$ represents the body force due to the gravity, and f_D Is the Darcy friction factor, which describes the pressure drop due to the viscous shear.

Between all the existing Darcy friction factor models in the literature Joseph and Yang [24], [25] for single phase flow, the Churchill relation is more suitable to describe the water. This relation is valid for laminar flow, turbulent flow, and transitional region in between. In the Churchill relation, the Darcy friction factor, where A and B are constants.is formulated as:

$$f_D = \left[\left(\frac{8}{Re}\right)^{12} + (A+B)^{-1,5}\right]^{\frac{1}{12}} \tag{11}$$

$$A = \left[-2.457 \ln\left(\frac{7}{Re}\right)^{0.9} + 0.27\left(\frac{e}{d_h}\right)\right]^{\frac{1}{12}} \tag{12}$$

$$B = \left(\frac{37530}{Re}\right)^{16} \tag{13}$$

The Reynolds number is equal to:

$$Re = \frac{\rho v d_h}{\mu} \tag{14}$$

where μ(Pa.s)the dynamic viscosity and e(m) is the surface roughness. The surface roughness is a function of the cooling channel material.

The energy equation for the cooling channel flow is:

$$\rho A C_p \frac{\partial T}{\partial t} + \rho A C_p v.\Delta T = \nabla\left(A\lambda \nabla T\right) + f_D \frac{\rho A}{2d_h} |v|^3 + Q_{wall} \tag{15}$$

where $C_p\left(\mathrm{jkg^{-1}K^{-1}}\right)$ the specific heat capacity of the water ethylene glycol is, $\lambda\left(\mathrm{Wm^{-1}K^{-1}}\right)$ is the thermal conductivity of the water ethylene glycol, the second term on the left hand corresponds to the heat dissipated due to viscous shear. Q_{wall} (W/m) is the heat transferred from the cold plate to the water ethylene glycol in the cooling channel through its wall is expressed as:

$$Q_{wall} = h_{int} Z (T_{wall} - T) \tag{16}$$

Where Z (m) is the wetted perimeter of the cooling channel, h_{int}(W/m^{2}K is an overall heat transfer coefficient between the internal film of the cooling channel and the wall of the cold plates, T_{wall} (°C) is the external temperature

outside of the mini-channel given by the 3D heat transfer in the cold plate, h_{int} has been estimated from the forced convection correlation, which depends on the Nusselt number (N_u) and Prandtl numbers (P_r), the flow regime and design of the channel. For laminar flow regime with round pipes [26]

For turbulent flow regime, the following Nusselt correlation has been used [27]:

$$Nu_{turb} = \frac{(f_D/8)(Re - 1000)Pr}{1 + 12.7\sqrt{f_d/8}(Pr^{2/3} - 1)} \tag{17}$$

The Prandtl number is expressed as:

$$Pr = \frac{\mu C_p}{\lambda} \tag{18}$$

h_{int} is expressed as:

$$h_{int} = Nu\frac{\lambda}{d_h} \tag{19}$$

With:

$$Nu = max\,(Nu_{lam}, Nu_{turb}) \tag{20}$$

4.3. Boundary and initial conditions

For the interface battery pack/cooling plates, the heat flux continuity is applied, where the heat from the battery is transferred to the cold plate:

$$-\lambda_{packbattery}\nabla T|_{boundaries} = -\lambda_{coldplate}\nabla T|_{boundaries} \tag{21}$$

At the interface between the cold plate and cooling channel, the boundaries conditions are given by the continuity of the heat transfer fluxes. Indeed the heat from the cold plates is transferred to the channels:

$$\lambda_{coldplate}\nabla T|_{boundaries} = Q_{wall} \tag{22}$$

At the inlet of the cooling channel, a temperature of T_{inlet} (°C) is specified:

At the outlet of the cooling channel, an outflow condition is applied. At the external surface, the heat is dissipated through the ambient air by convection:

$$\lambda\nabla T|_{boundaries} = h_{ext}(T - T_{amb}) \tag{23}$$

h_{ext} (W/m^2 K) is the convective heat coefficient between the interface battery and cooling plates included and ambient environment. T_{amb}(°C) is the ambient air temperature. The initial temperature of the battery pack is defined as T_{ini}(°C):

In the inlet, the liquid velocity is equal to the ratio of volumetric flow rate and the cross-section of the cooling channel (see Table 2).

$$v = \frac{q_{v,0}}{A} \tag{24}$$

$q_{v,0}$(m^3/s) is volumetric flow rate. In the outlet, the atmospheric pressure ($p_a\,(Pa)$) is assigned $p = p_a$

4.4. Results and discussion

All equations are simultaneously solved numerically in ANSYS FLUENT by using the Finite Element's Method. However, the unstructured mesh was generated by using the ANSYS Meshing software, with refining zones at the cooling channels zones. The temperature is solved by using the SIMPLE Solver Algorithm. For each time step, the convergence is reached where the relative tolerance is below 10^{-3} for all variables.

The simulation of the different cooling plate design is performed by using the same conditions, physical and cooling parameters. The impact of the cold plate's designs on the battery pack behaviour is investigated by considering the heat removed by the refrigerant and the heat dissipated through the ambient air with convective coefficient of 100 W/m^{2}K. The water ethylene glycol is used as a refrigerant with a volume flow rate of 1 kg/s and an inlet and initial temperature of 288 °K.

Table 2. Thermal parameters for the investigation.

Material proprieties	Value
Coolant fluid	Water-ethylene-glycol
Coolant viscosity (Pa s)	0.00315
Coolant conductivity ($Wm^{-1}k^{-1}$)	0.419
Coolant specific heat ($JKg^{-1}k^{-1}$)	3494
Coolant density ($Kg\,m^{-3}$)	1065
Plate material	Aluminium
Plate conductivity ($Wm^{-1}k^{-1}$)	202
Plate specific heat ($JKg^{-1}k^{-1}$)	871
Plate density (Kgm^{-3})	2719
Channel material	Copper
Channel conductivity ($Wm^{-1}k^{-1}$)	390
Channel specific heat ($JKg^{-1}k^{-1}$)	390
Channel density (Kgm^{-3})	8900

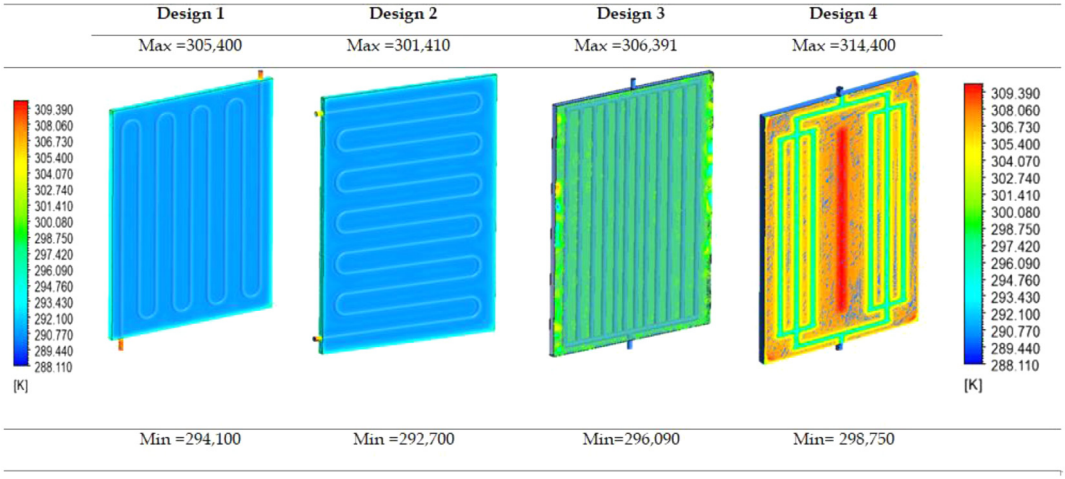

Fig. 8. Temperature distribution over different cold plate designs at $T_{inlet} = 290\ ^{\circ}K$ and $T_{ambiant} = 300^{\circ}$ with $h = 100\ \mathrm{W}\left(\mathrm{m}^2\mathrm{K}\right)$.

The Fig. 8 clearly shown that the cooling plate's designs give different temperature profile trends. The results indicate more temperature drops with the design 2, follow by design 1, design 3 and design 4. Due to the division of the flow rate in the different channel branches of the design 3 and design 4, less temperature drops are observed, compared to the designs 1 and 2, for which the flow rate remains the same and is equal to its total value. In conclusion, as the difference between the maximum temperatures given by the different cold plate design is low, our main criteria of selection are dictated by the design with the lowest temperature gradient. Therefore, the design 1 is identified to be more appropriate to build an efficient external cooling plate for the battery pack.

In fact, in the following Fig. 9 we see clearly the impact of the cold plate on the battery pack which can decrease the temperature at 30 °C which is the best recommended value for the battery pack.

5. Conclusion

A 3D-thermal model is developed for Li-ion battery pack for EVs, which is able to investigate and to analyse the temperature distribution of the battery at discharging conditions. The ANSYS FLUENT software has been used to solve the model development. The simulation result show that the battery surface temperature is nearly uniform, except in the middle where the maximum temperature is located (48 °C). This value is higher than the recommended operation value in the charging state which means that an external cooling system is required to reduce it. Moreover, different liquid cold plate's configurations have been investigated in order to obtain the efficient cooling architecture, which allows to decrease the temperature and to obtain a more uniform temperature distribution over the surface

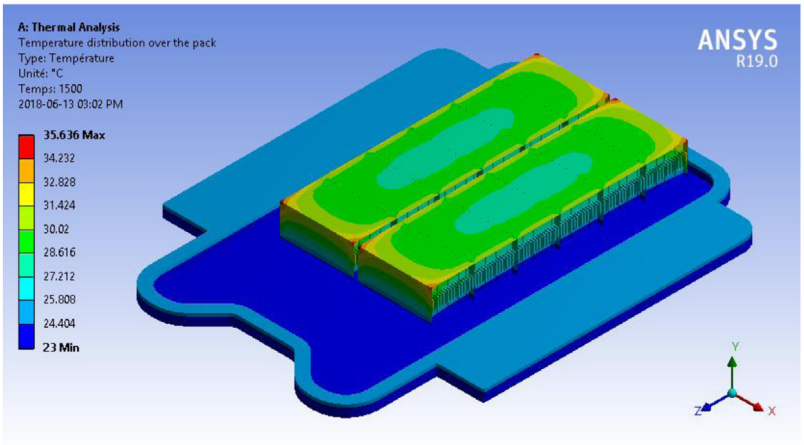

Fig. 9. Influence of the cold plate on the battery pack.

of the battery pack. It has been found that the cooling plate with (design 2) successfully controls the maximum temperature and reduces the temperature gradient due to the high surface contact between the cooling channel and plates. Furthermore, the optimization of the operating conditions for this solution has been calculated for a flow rate of 1.5 kg/s at inlet temperature of 15 °C. These values represent an optimum for lowering the maximum temperature increase. Finally, the required pump power needed is about 1 Kw for efficient cooling of the investigated pack battery. Future work will focus on the optimization of the cold plate. And its operating conditions.

References

[1] Ehsani M, Gao Y, Emadi A. Modern electric, hybrid electric, and fuel cell vehicles: fundamentals, theory, and design. CRC Press; 2010.

[2] Amjad S, Neelakrishnan S, Rudramoorthy R. Review of design considerations and technological challenges for successful development and deployment of plug-in hybrid electric vehicles. Renew Sustain Energy Rev 2010;14:1104–10. http://dx.doi.org/10.1016/j.rser.2009.11.001.

[3] Greco A, Jiang X, Cao D. An investigation of Lithium-Ion battery thermal management using paraffin/porous-graphite-matrix composite. J Power Sources 2015;278:50–68. http://dx.doi.org/10.1016/j.jpowsour.2014.12.027.

[4] Waag W, Käbitz S, Sauer DU. Experimental investigation of the Lithium-Ion battery impedance characteristic at various conditions and aging states and its influence on the application. Appl Energy 2013;102:885–97. http://dx.doi.org/10.1016/j.apenergy.2012.09.030.

[5] Ramadass P, Haran B, White R, Popov BN. Capacity fade of Sony 18 650 cells cycled at elevated temperatures Part I. Cycling performance.

[6] Uchida I, Ishikawa H, Mohamedi M, Umeda M. AC-impedance measurements during thermal runaway process in several Lithium/polymer batteries. J Power Sources 2003;119–121:821–5. http://dx.doi.org/10.1016/S0378-7753(03)00248-9.

[7] Jhu C-Y, Wang Y-W, Wen C-Y, Shu C-M. Thermal runaway potential of $LiCoO_2$ and $Li(Ni1/3Co1/3Mn1/3)O_2$ batteries determined with adiabatic calorimetry methodology. Appl Energy 2012;100:127–31. http://dx.doi.org/10.1016/j.apenergy.2012.05.064.

[8] Lin H-p, Chua D, Salomon M, Shiao H-C, Hendrickson M, Plichta E, et al. Low-temperature behavior of Li-Ion cells. Electrochem Solid-State Lett 2001;4:A71. http://dx.doi.org/10.1149/1.1368736.

[9] Bandhauer TM, Garimella S, Fuller TF. A critical review of thermal issues in Lithium-Ion batteries. J Electrochem Soc 2011;158:R1. http://dx.doi.org/10.1149/1.3515880.

[10] Khan M, Swierczynski M, Kær S. Towards an ultimate battery thermal management system: A review. Batteries 2017;3:9. http://dx.doi.org/10.3390/batteries3010009.

[11] Lu L, Han X, Li J, Hua J, Ouyang M. A review on the key issues for Lithium-Ion battery management in electric vehicles. J Power Sources 2013;226:272–88. http://dx.doi.org/10.1016/j.jpowsour.2012.10.060.

[12] Benabdelaziz K, Maaroufi M, Ikken B. Degradation of Lithium-Ion batteries in electric vehicles at high temperatures: A case study. 2018, http://dx.doi.org/10.1109/IRSEC.2018.8702871.

[13] Barré A, Deguilhem B, Grolleau S, Gérard M, Suard F, Riu D. A review on Lithium-Ion battery ageing mechanisms and estimations for automotive applications. J Power Sources 2013;241:680–9. http://dx.doi.org/10.1016/j.jpowsour.2013.05.040.

[14] Omar N, Gualous H, Salminen J, Mulder G, Samba A, Firouz Y, et al. Electrical double-layer capacitors: evaluation of ageing phenomena during cycle life testing. J Appl Electrochem 2014;44:509–22. http://dx.doi.org/10.1007/s10800-013-0640-4.

[15] Omar N, Monem MA, Firouz Y, Salminen J, Smekens J, Hegazy O, et al. Lithium Iron phosphate based battery - Assessment of the aging parameters and development of cycle life model. Appl Energy 2014;113:1575–85. http://dx.doi.org/10.1016/j.apenergy.2013.09.003.

[16] Smith J, Hinterberger M, Hable P, Koehler J. Simulative method for determining the optimal operating conditions for a cooling plate for Lithium-Ion battery cell modules. J Power Sources 2014;267:784–92. http://dx.doi.org/10.1016/j.jpowsour.2014.06.001.
[17] Jarrett A, Kim IY. Design optimization of electric vehicle battery cooling plates for thermal performance. J Power Sources 2011;196:10359–68. http://dx.doi.org/10.1016/J.JPOWSOUR.2011.06.090.
[18] Jin LW, Lee PS, Kong XX, Fan Y, Chou SK. Ultra-thin minichannel LCP for EV battery thermal management. Appl Energy 2014;113:1786–94. http://dx.doi.org/10.1016/j.apenergy.2013.07.013.
[19] van Gils RW, Danilov D, Notten PHL, Speetjens MFM, Nijmeijer H. Battery thermal management by boiling heat-transfer. Energy Convers Manage 2014;79:9–17. http://dx.doi.org/10.1016/J.ENCONMAN.2013.12.006.
[20] Perner A, Vetter J. Lithium-Ion batteries for hybrid electric vehicles and battery electric vehicles. 2015.
[21] Gu WB, Wang CY. Thermal-electrochemical modeling of battery systems. J Electrochem Soc 2000;147:2910. http://dx.doi.org/10.1149/1.1393625.
[22] Inui Y, Kobayashi Y, Watanabe Y, Watase Y, Kitamura Y. Simulation of temperature distribution in cylindrical and prismatic Lithium Ion secondary batteries. Energy Convers Manage 2007;48:2103–9. http://dx.doi.org/10.1016/J.ENCONMAN.2006.12.012.
[23] Samba A. Battery Electrical Vehicles-Analysis of Thermal Modelling and Thermal Management. LUSAC (Laboratoire Universitaire des Sciences Appliquées de Cherbourg), Université de caen Basse Normandie; MOBI (the Mobility, Logistics and Automotive Technology Research Centre), Vrije Universiteit Brussel. 2015.
[24] Joseph DD, Yang BH. Friction factor correlations for laminar, transition and turbulent flow in smooth pipes. Physica D 2010;239:1318–28. http://dx.doi.org/10.1016/J.PHYSD.2009.09.026.
[25] Teruel FE, Rizwan-uddin. Characterization of a porous medium employing numerical tools: Permeability and pressure-drop from Darcy to turbulence. Int J Heat Mass Transfer 2009;52:5878–88.
[26] Incropera FP, DeWitt DP, Bergman TL, Lavine AS. Fundamentals of Heat and Mass Transfer, US Patent 5, 328, 671. http://dx.doi.org/10.1073/pnas.0703993104.
[27] Bianchi A, Fautrelle Y, Etay J, Longchamp R. Transferts thermiques, presses polytechniques et universitaire Romandes, Lausanne. ISBN: 9782880744960. 2004.